

Arginine-rich cell-penetrating peptides induce membrane multilamellarity and subsequently enter via formation of a fusion pore

Christoph Allolio^{1a,b,c}, Aniket Magarkar^{1a,d}, Piotr Jurkiewicz^e, Katarina Baxova^a, Matti Javanainen^a, Philip E. Mason^a, Radek Šachl^e, Marek Cebecauer^e, Martin Hof^e, Dominik Horinek^b, Veronika Heinz^f, Reinhard Rachel^g, Christine Ziegler^{f,h}, Adam Schröfelⁱ, and Pavel Jungwirth^{2a}

^aInstitute of Organic Chemistry and Biochemistry, Czech Academy of Sciences, Flemingovo nám. 2, CZ-166 10 Prague 6, Czech Republic; ^bInstitut für Physikalische und Theoretische Chemie Universität Regensburg, 93040 Regensburg, Germany; ^cFritz Haber Institute for Molecular Dynamics and Department of Chemistry, The Hebrew University of Jerusalem Edmond J. Safra Campus, Giv'at Ram, Jerusalem 9190401, Israel; ^dFaculty of Pharmacy, University of Helsinki, Viikinkaari 5E, Helsinki 00014, Finland; ^eJ. Heyrovský Institute of Physical Chemistry, Czech Academy of Sciences, v.v.i., Dolejškova 2155/3, 182 23 Prague 8, Czech Republic; ^fInstitute of Biophysics and Biophysical Chemistry, University of Regensburg, Regensburg, Germany; ^gLehrstuhl für Mikrobiologie und Archaeenzentrum, Universität Regensburg, Universitätsstrasse 31, D-93053 Regensburg, Germany; ^hInstitute of Biophysics and Biophysical Chemistry, University of Regensburg, Regensburg, Germany; ⁱMIMCF at BIOCEV, Faculty of Sciences, Charles University Prumyslová 595, Vestec, 242 50, Czech Republic

This manuscript was compiled on September 30, 2018

1 **Arginine-rich cell penetrating peptides do not enter cells by directly**
2 **passing through a lipid membrane, they instead passively enter vesicles**
3 **and live cells by inducing membrane multilamellarity and fusion.**
4 **The molecular picture of this penetration mode, which differs qualitatively**
5 **from the previously proposed direct mechanism, is provided by**
6 **molecular dynamics simulations. The kinetics of vesicle agglomeration**
7 **and fusion by an iconic cell penetrating peptide - nonaarginine**
8 **- is documented via real time fluorescence techniques, while the induction**
9 **of multilamellar phases in vesicles and live cells is demonstrated by a combination**
10 **of electron and fluorescence microscopies. This concert of experiments and simulations**
11 **reveals that the newly identified passive cell penetration mechanism bears analogy to vesicle**
12 **fusion induced by calcium ions, indicating that the two processes may share a common**
13 **mechanistic origin.**

Cell penetrating peptides | Vesicle fusion | Ion membrane interactions |
Molecular dynamics | Fluorescence microscopy | Electron microscopy

1 Cell penetrating peptides have a unique potential for targeted drug delivery, therefore, mechanistic understanding of their membrane action has been sought since their discovery over 20 years ago.(1) While ATP-driven endocytosis is known to play a major role in their internalization(2), there has been also ample evidence for the importance of passive translocation(3–5) for which the direct mechanism, where the peptide is thought to directly pass through the membrane via a temporary pore, has been widely advocated. (4, 6–8) Here, we question this view and show that arginine-rich cell penetrating peptides instead passively enter vesicles and live cells by inducing membrane multilamellarity and fusion.

13 Ions do not dissolve in oil. From this point of view the direct passive mechanism of cell penetration is intuitively problematic, as cationic peptides such as polyarginines or the trans-activating transcriptional activator (TAT) are too highly charged to be able to pass through the "oily" interior of a lipid membrane. The concept of direct penetration was seen plausible due to the action of the related antimicrobial peptides, which are also charged, but in addition contain a large fraction of hydrophobic residues(9): These peptides are known to stabilize pores in membranes(10). At a close inspection, however, it becomes clear that their charged sidechains do not interact directly with the aliphatic chains in the low dielectric interior of the phospholipid bilayer, but rather stabilize tran-

26 sient water channels or act as terminal residues anchoring the transmembrane helix.(9) Taken together, the passive action of cell penetrating peptides (CPP) seems to be very different from direct translocation across an otherwise unperturbed cell membrane.

31 To make matters even more confusing, experimental facts and suggested mechanisms often seem contradictory to each other. For example, there are conflicting reports whether or not nonaarginine (R₉) is able to penetrate vesicles composed purely of 1-palmitoyl-2-oleoyl-phosphatidylcholine (POPC). (5, 11, 12) Additionally, fluorescence microscopy suggests that R₉ is able to deform membranes(5, 13) and small angle X-ray scattering (SAXS) experiments reveal phase transitions induced in lipid systems by polyarginines.(4) An important factor in these observations appears to be the membrane composition with negatively charged lipids facilitating membrane translocation of cationic peptides.(7, 14) Indeed, there is some evidence that a direct mechanism may be enabled by hydrophobic counterions, such as pyrene butyrate(12, 15) or presence of an unphysiological concentration of phosphatidic acids.(7) The relevance to of these phenomena to actual cellular uptake is not clear, so that current discussions present direct mechanisms

Significance Statement

The passive translocation mechanism of arginine-rich cell penetrating peptides has puzzled the scientific community for more than twenty years. In this study we propose a new mechanism of passive cell entry involving fusion of multilamellar structures generated by the cell penetrating peptides. The geometry of entry for this mechanism is completely different from previously suggested direct translocation mechanisms leading to a new paradigm for designing molecular carriers for drug delivery to the cell.

A.M., C.A. and M.J. performed the simulations, supervised by P.Jun and D. H., vesicle fluorescence related experiments and DLS were performed by P.Jur., C.A., K.B. and supervised by M. H. fluorescence data were interpreted by C.A. and R.S. Cryoelectron microscopy on LUVs was performed by V.H. and R.R., supervised by C.Z.; fluorescence and electron microscopy on HeLa cells was done by M.C., A.S. and P.E.M.; simulation visualizations were done by A.M. and C.A.; C.A. and P.Jun wrote the paper.

The authors declare no competing financial interests.

¹C.A. and A.M. contributed equally to this work

²To whom correspondence should be addressed. E-mail: pavel.jungwirth@marge.uochb.cas.cz.

side by side with endocytosis-like membrane deformations induced by the CPP.(16)

Another fundamental cellular process involving membranes and charged species is fusion of vesicles with the cell membrane during calcium-triggered exocytosis. In cells, vesicle-membrane fusion is mediated by the SNARE protein complex(17, 18) with synaptotagmins(19), nevertheless, it can also be induced in *in vitro* lipid vesicles without the need for the presence of the protein machinery(20, 21). It is experimentally well established that Ca^{2+} is a key player capable of promoting vesicle fusion(22) and there is general consensus about the fusion mechanism, which proceeds via a stalk intermediate, followed by formation of a hemifused structure and opening of a fusion pore.(23, 24) In this context, it is worth mentioning that cationic cell penetrating peptides, especially TAT and its derivatives, are known to aggregate at phospholipid membranes and occasionally fuse vesicles.(2, 5, 20, 25) This brings up the idea, which is examined further in this study, that the processes of passive cell penetration and membrane fusion may be mechanistically more intimately connected than thought so far.(25)

Results and Discussion

Exploring vesicle penetration by a fluorescence leakage assay. In order to explore the potential connection between cell penetration and membrane fusion, we start by investigating the abilities of R_9 as an archetypal CPP, in contrast to non-CPPs like tetraarginine (R_4) or nonalysine(26) (K_9), to penetrate and cause leakage of large unilamellar vesicles (LUVs) of varying lipid compositions using a fluorescence leakage assay (for details see Methods and the SI Appendix). While, contrary to some published data(12), pure POPC LUVs do not show leakage upon exposure to R_9 even at high peptide concentrations, LUVs composed of mixtures of 1,2-dioleoyl-phosphatidylethanolamine (DOPE) and 1,2-dioleoyl-phosphatidylserine (DOPS) exhibit leakage as long as the content of DOPE is sufficiently high (see Table S3 in the SI Appendix). Despite different lipid composition of the present vesicles compared to live cells, we did recover the arginine ‘magic’, i.e., the high activity of CPPs with more than about seven aminoacids and high arginine content (27). In these vesicles, similarly to experiments in cells, R_9 was always found to be an efficient leakage agent, in contrast to K_9 or R_4 (see Figure 1, top left). Using dynamic light scattering (DLS) measurements we showed that leakage is accompanied with vesicle aggregation, as the leakage kinetics mimics the increase in time of the mean diameter of the aggregates (see Figure 1, top right and the SI Appendix, Table S3 for the DOPE-rich lipid composition).

Membrane fusion induced by calcium as well as by cationic cell penetrating peptides. The range of lipid compositions of vesicles capable of being leaked by R_9 is at odds with simulations of direct translocation, where a far higher translocation free energy has been predicted for DOPE-rich bilayers than for those rich in POPC.(28) However, it seems to match compositions known to enhance vesicle fusion by calcium.(20, 21, 29) Both PE and PS (as well as several other anionic lipids) are fusogenic in presence of Ca^{2+} .(30–32) In order to verify this correlation, we repeated the experiments with Ca^{2+} instead of R_9 . Indeed, we were able to observe calcium-induced leakage

for lipid compositions that were most susceptible to leakage by the CPPs as well (see Table S3 in the SI Appendix). In order to obtain a comparable effect, however, the concentration of Ca^{2+} had to be significantly higher than that of R_9 , even when taking into account the significantly larger charge carried by the latter species.

At high peptide content, the LUV leakage kinetics is described *quantitatively* by a second order rate law in the vesicle concentration (for details see Figure S11 and the kinetic model in the SI Appendix). This indicates that aggregation of vesicles and the double bilayer formed during this process is essential for vesicle leakage. It is indicative that for all lipid compositions at which significant leakage occurs the vesicles also exhibit R_9 -induced fusion, as detected by a near complete lipid mixing in a Förster resonance energy transfer (FRET) assay (see the SI Appendix, esp. Figure S11). Moreover, the leaky lipid compositions are those known to be susceptible to Ca^{2+} mediated fusion. Note that leaky fusion has been observed previously in conjunction with cell penetrating peptides and has even been used to classify them.(25) In addition to the above circumstantial evidence for a direct connection between cell penetration and membrane fusion we add further experimental support using confocal microscopy finding agglomeration of giant unilamellar vesicles (GUVs) together with leakage (see Figure 1). We were able to observe fusion of GUVs directly (see the Supporting Video) and, using Oregon Green 488 (OG)-labeled peptides, we confirmed a preferential adsorption of fluorescently labeled R_9 to the vesicles (see Figure S8 in the SI Appendix). Finally, adding Ca^{2+} instead of R_9 to the GUVs we found a functionally analogous behavior (see the SI Appendix).

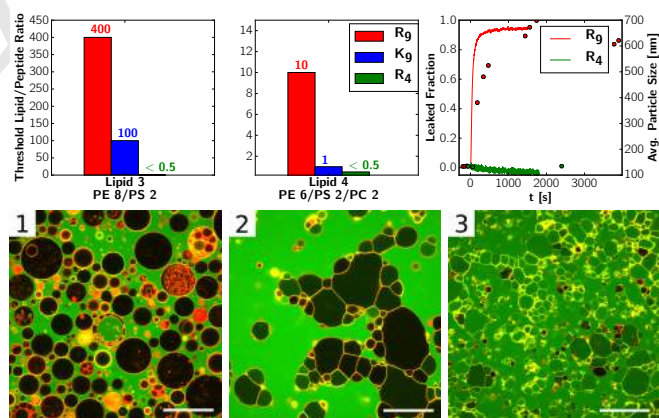


Fig. 1. Fluorescence spectroscopy results. Top Left: Threshold concentrations for leakage induced by R_9 , K_9 and R_4 given as inverse of the peptide/lipid ratios for two lipid compositions: DOPE/DOPS 80/20 (3) and DOPE/DOPC/DOPS 60/20/20 (4) (the higher the threshold value, the more efficient the peptide is in leaking the vesicles). Top Right: DLS measurements showing particle growth (right axis, dots) overlaid with leakage kinetics (left axis, lines) for R_9 for the composition (3) and absence of particle growth and leakage for R_4 . Bottom panel: Fluorescence microscopy images showing the effect of R_9 on GUV with composition (4). From left to right: 1. No peptide added, 2. Shortly after addition of R_9 3. Final state after 1h. Bars = 50 μm .

Ideal fusion topologically precludes cell penetration. The similarities in aggregation/fusion caused by R_9 and Ca^{2+} are illustrated in Figure 2, A–J. In the context of the present study, it is important to note that there is no topological way for peptides to enter the vesicles from the outside (or do the reverse) by an ideal fusion process, within which two unilamellar vesicular structures coalesce, as it merely connects the

145 interiors of the two vesicles. A previous electron microscopy
 146 study of Ca^{2+} -mediated fusion reported content loss along the
 147 fusion diaphragm, attributing it to the strain induced by the
 148 deformation during agglomeration.(33). A close observation
 149 of the GUVs in Figure 1 indeed reveals that they are signifi-
 150 cantly deformed as the agglomeration creates nearly planar
 151 surfaces at the regions of contact, indicating high tension.
 152 While tension supports several fusion steps (34), the large
 153 surface tension of the agglomerated, flat, and fusing double
 154 bilayers can lead to rupture - depending on the initial tension
 155 of the vesicles it may overcome the line tension leading to a
 156 membrane pore. However, a small, transient, pore near the
 157 fusion stalk can hardly be the main mechanism of penetration
 158 of peptides into vesicles since it will rapidly close (35, 36),
 159 making it hard for cargo to pass through. Such pores are
 160 also associated with positive curvature, as induced by certain
 161 amphipathic helices(37), whereas we stabilize fusion stalk and
 162 pore with PE lipids (23) inducing negative curvature and the
 163 hydrophilic R_9 . For a cell membrane to be ruptured a large
 164 enough membrane fold for self-fusion would have to be gener-
 165 ated first. This is only possible for a system without a large
 166 surface tension. However, such membranes are unlikely to be
 167 ruptured by a fusion event. Therefore, rupture cannot explain
 168 continuous leakage into intact vesicles, nor is it a plausible
 169 mechanism for cell penetration as cells tightly regulate their
 170 inner pressure and membrane tension and are rich in chole-
 171 sterol, which increases pore line tension. We show below that
 172 a solution lies in locally bifurcating the membrane, leading to
 173 multilamellar structures. Such a pathway allows the peptides
 174 to enter by fusion without having to form transient pores, as
 shown schematically in Figure 2, K-V.

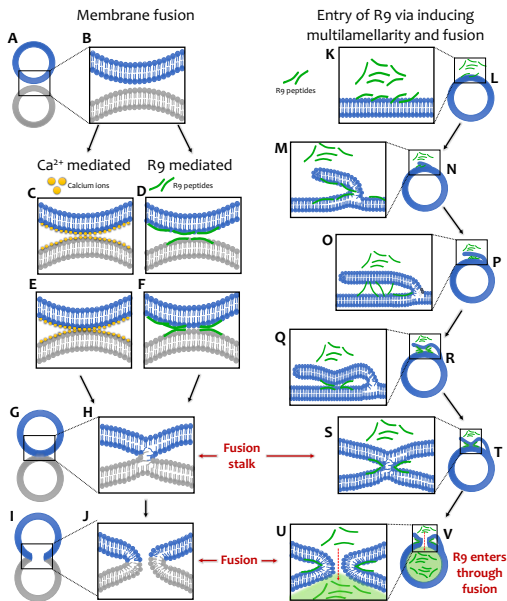


Fig. 2. The schematic mechanisms of R_9 and Ca^{2+} mediated vesicle fusion: **A** Fusion of different vesicles (in blue and grey), by **B** interface contact. **C, D** Adsorption of the charged particles (R_9 in green and Ca^{2+} in yellow). **E, F** Agglomeration of the bilayers induced by crosslinking. **G** Stalk formation. **H** Opening of the fusion pore. **I, J** R_9 translocation via self-fusion of a single vesicle. **K-V** starting from a flat vesicle surface bilayer. **K** Strong adsorption of R_9 . **L, M** Membrane bifurcation through adhesion and curvature. **M, N** Extension of the bifurcated bilayer through R_9 crosslinking **O, P**. Agglomeration of the bilayers induced by crosslinking of two bilayers on the same vesicle **Q, R**. Stalk formation **S, T** and opening of the fusion pore through which additional R_9 peptides enter **U, V**.

Induced multilamellarity as a solution to the topological conundrum.

Cryo-electron microscopy: Seeing is believing. A tendency of GUVs(13) or cells(12) to become multilamellar upon addition of CPPs has been observed recently. To further explore this idea, we first conducted cryo-EM experiments on LUVs. The obtained cryo-EM images indeed reveal formation of multilamellar domains and lipid bilayer bifurcations after the addition of R_9 , see Figure 3. Additional time-resolved FRET experiments on fluorescently labeled LUVs reveal presence of inter-bilayer energy transfer, which provides independent confirmation for the induction of multilamellar lipid structures by R_9 (see the SI Appendix and Figure S11 therein). Importantly, Ca^{2+} ions are also able to fuse and collapse vesicles to multilamellar phases due to the ability of Ca^{2+} to bridge phosphates from different bilayers.(33) The cryo-EM structures also provide some additional evidence for fusion, as the LUVs in Figure 3, A are many times larger than those found in the initial state (again see Figure S7, A).

Multilamellar structures can be formed via folding of a membrane or by stacking of deflated vesicles. Any process based on direct membrane stacking would, however, add an even number of bilayers in between the vesicles and, therefore, would not lead to leakage via fusion. It is thus a key finding that by counting the lipid bilayers we frequently find odd numbers (see Figure 3, D). Moreover, a close inspection of the EM micrographs provides direct evidence for bilayer bifurcation at multiple positions (see Figure 3, C for an example). We conclude that R_9 is indeed capable of inducing multilamellarity by membrane adsorption and bifurcation, rendering a cell penetration mechanism via fusion feasible.

The proposed mechanism shares some similarities with the reverse micelle mechanism, proposed in the literature(38, 39). This mechanism also necessitates a small bifurcation, before the membrane edge is closed by forming the reverse micelle. The reverse micelle has negative curvature on the inside and is, therefore, stabilized by similar interactions as the bifurcations. We argue that the membrane edge energy can be compensated through extension of stable cross-linked multilamellar domains as seen in the EM pictures. In the SI we show simulations, which indicate the stabilization of the bifurcation by R_9 , but not R_4 even in the absence of crosslinking. The opening of a reverse micelle removes negative curvature from the system. In contrast to this, the fusion stalk(23) and pore both maintain a negative curvature – a finite bilayer thickness translates negative Gaussian curvature into negative mean curvature, present on both membrane leaflets.(40) Thereby the whole mechanism can be driven by the same preferential interaction with R_9 .

Fluorescence and electron microscopy on HeLa cells. In order to directly explore the mechanism behind cellular uptake of CPPs in the absence of endocytosis, we first observed penetration into living human HeLa cells by fluorescence confocal microscopy (Figures S9, S10 in the SI Appendix). HeLa cells incubated with $15 \mu\text{M}$ Oregon-Green (OG) labeled- R_9 peptide for 3 minutes at 4°C already exhibited surface fluorescence and, in particular, the presence of highly fluorescent foci (SI Appendix, Figure S9, arrows). Longer incubation of cells with the peptide increased the number of foci detected on HeLa cells. Cytosolic presence of the peptide was observed as soon

175

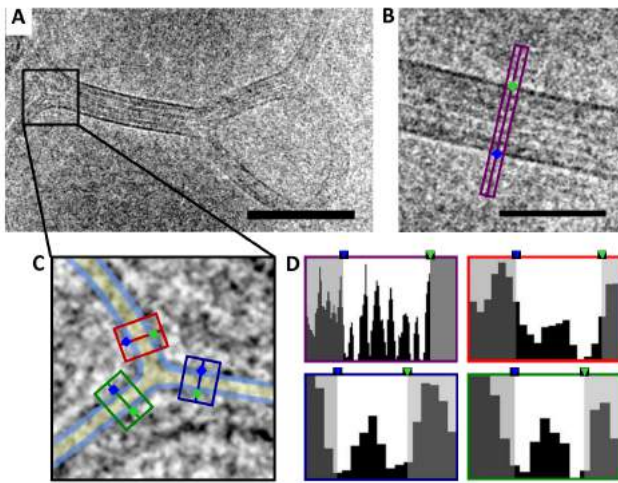


Fig. 3. Electron micrographs of LUVs in the presence of R_9 . (A): vesicles treated with R_9 (>60 sec.) fuse with each other and exhibit bifurcated, multilamellar membranes; Bar = 100 nm. (B) Example of a multilamellar membrane. Bar = 50 nm.; The violet box is analyzed in (D). (C): Example of a membrane bifurcation. The membranes before and after the bifurcation site are analyzed by line-scans. The line-scan areas are marked with colored boxes. (D): The histograms are boxed in the same color as the respective line-scan areas in (B) and (C). The histogram (upper left panel) corresponding to the multilamellar membrane (shown in (B)) exhibits seven distinct minima attributed to individual membranes.

cell membrane also points to a yet unknown specific interaction which is not present in the synthetic vesicle systems.

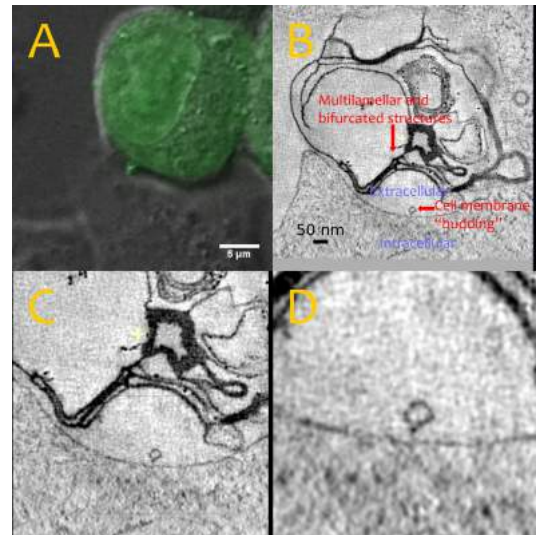


Fig. 4. Electron microscopic and fluorescence microscopy images of the same spot on a fixated HeLa cell in the presence of OG- R_9 . (A): A fluorescence microscopy image of the multilamellar spot showing the presence of the labeled peptide. (B-D): An electron microscopy image at three zooms exhibiting bifurcated, multilamellar membranes and vesicle budding. (C) An example of a multilamellar membrane structure.; (D): Focus on a budding protrusion.

236 as 5 min after addition of the peptide to the cells and the number of penetrated cells increased over prolonged incubation time (even when cells were washed after 3 minutes to remove free peptide from incubation medium). All cells with cytosolic peptide exhibited at least 1-2 fluorescent foci on their surfaces. Moreover, these foci were found only in cells with exocytosis blocked by low temperature.

243 These results suggest that R_9 rapidly accumulates in a very few places on a cell at low temperatures. Previously, electron microscopy (EM) on cells revealed that addition of R_9 leads to the formation of layered membrane domains.(41) Motivated by these observations, we performed EM experiments on HeLa cells with added fluorescently labeled R_9 . In accord with our observations on vesicles and with previous EM on cells(41) we see regions of protrusions, bifurcations, and multilamellarity by incubating cells with R_9 at 4 °C. At these conditions active endocytosis is switched off and only passive cell penetration is operational (see Figure 4, B). The branched structures (see zoomed-in images in Figure 4, C) are topologically identical to those suggested in the schematic drawing above (Figure 2, M) and to the structures observed in the LUVs (Figure 3). The observed protrusions indicate that a strong curvature-generating interaction is at work, as can be seen in Figure 4, D. Specifically, we interpret the budding spherical protrusions as being due to negative (Gaussian) curvature generation, similar as occurring in a fusion stalk. By overlaying fluorescence images with EM we clearly see that the changes in the bilayer structure correlate with the location of the fluorescently labeled OG- R_9 , as can be seen in Figure 4, A. Our EM images on HeLa cells are thus consistent with the above results on vesicles, as well as with previous observations showing that giant plasma membrane vesicles (GPMVs) are susceptible to R_9 penetration, but only in the presence of intact membrane proteins.(3) Note that in contrast to our leakage experiments on LUVs the local, encapsulated foci will allow only very limited diffusion, thereby limiting potential cell toxicity of the CPP. Their locality at the

Molecular dynamics simulations: Atomistic insights. In order to gain atomistic insight into the fusion process and its connection to cell penetration we performed molecular dynamics simulations. Previous studies, based on continuum and coarse-grained models agree that fusion proceeds via a stalk intermediate. (23, 35) The stalk is strongly concave, explaining the observed lipid selectivity toward small (PE) headgroups as these stabilize negative curvature.

Our simulation setups involve strongly positively curved bilayer geometries, intended to lower the barriers for fusion.(42, 43) The stress hereby induced in the PE-rich bilayers leads to spontaneous stalk formation in our Simulations (see Methods and the SI Appendix for full details). Snapshots from the R_9 or Ca^{2+} mediated fusion processes are presented in Figure 5. We find both Ca^{2+} ions and the charged R_9 side chains to bind to lipid headgroups, primarily at the negatively charged phosphates. Subsequently, we observe mechanistic similarities in the membrane fusion mediated by Ca^{2+} and R_9 . The first step in the fusion process is crosslinking, i.e., simultaneous binding of lipids from two membrane bilayers by either Ca^{2+} or R_9 , with the latter being found to be a particularly effective crosslinker. As the ions keep the bilayers in close contact, the lipid tails eventually crosslink, too, in what appears to be the rate-determining step of the whole fusion process. This lipid tail crosslinking occurs within about half a microsecond. Once a cross-linking lipid tail has flip-flopped into the opposing bilayer, the stalk starts forming within a few nanoseconds (Figure 5, B and C).

In Figure 5, D we examine the action of R_9 on the membrane in close detail. First, we note the long-range crosslinking capability of R_9 , which is likely to be responsible for its strongly agglomerating effect on vesicles and for stabilizing the multilamellar structures we find in electron microscopy. R_9 tends to be only partially adsorbed at the membrane and can

308 thus easily reach across the interface and attach to the second
 309 bilayer. It is clear that for such a crosslinking a minimum
 310 chain length is necessary, which explains the inefficiency of
 311 R_4 in this respect (see also the control simulation data, in
 312 Figure S3 in the SI Appendix). In addition, R_9 also forms
 313 agglomerates when crosslinking the interfaces. It is known
 314 that R_9 binding to membranes is more cooperative than that
 315 of K_9 (44), making the former a much more efficient agent of
 316 membrane fusion and cell penetration than the latter. The
 317 attraction of R_9 to negatively charged lipids also leads to a
 318 lipid sorting effect, with phosphatidylserine lipids (Figure 5,
 319 D, orange) being accumulated next to the R_9 agglomerate.
 320 Electrostatics-based lipid sorting (involving, e.g., gangliosides)
 321 may contribute to the action in cells, membranes of which
 322 would otherwise not be sufficiently active. In the bottom
 323 right panel of Figure 5, we show that R_9 is preferentially ad-
 324 sorbed to regions of negative curvature(45) (marked by the
 325 color-coded surface), as this allows it to efficiently bind its
 326 sidechains to lipid headgroups (marked in gold). Aggregation
 327 of headgroups increases membrane tension in the headgroup
 328 region and exposes hydrophobic patches (visible in all panels
 329 of Figure 5, D). The exposure of hydrophobic patches in turn
 330 lowers hydration repulsion. Once lipid tails from opposing
 331 bilayers are in contact, lipid flip-flop can readily occur, starting
 332 thus the fusion cascade. At the surface of the fusion stalk and
 333 the pore, a very strongly negative Gaussian curvature and a
 334 negative mean curvature occur simultaneously. This stabili-
 335 zes the actual geometry and, therefore, lowers the barrier for
 336 fusion. The induction of negative Gaussian curvature has pre-
 337 viously been proposed as a characteristics of cell penetrating
 338 peptides.(4). Importantly for the present mechanism, we do
 339 not observe membrane rupture or water permeation during
 340 the fusion process.

341 Conclusions

342 In summary, we unraveled here a novel passive entry mecha-
 343 nism of cell penetrating peptides via branching and layering
 344 of membranes followed by fusion of the agglomerated systems.
 345 The layering is induced by a cooperative bridging of bilayers
 346 via adsorbed R_9 . The peptides also induce membrane bifurca-
 347 tions that allow to connect the vesicle exterior and interior via
 348 fusion and thus to translocate the cell penetrating peptides
 349 (which would not be topologically possible within an ideal
 350 vesicle fusion). The actual R_9 -induced fusion process then
 351 mirrors that of Ca^{2+} assisted vesicle fusion. The viability
 352 of this mechanism is supported by experimental results from
 353 electron microscopy, fluorescence microscopy, and light scatter-
 354 ing, together with with molecular dynamics simulations. The
 355 atomistic simulation data shed further light on the molecular
 356 mechanism of formation of the fusion stalk and pore. While the
 357 new mechanism has been unraveled for lipid vesicle systems,
 358 which allow for investigations with unprecedented molecular
 359 detail, induction of membrane branching and multilamellarity
 360 by polyarginines has been observed by electron microscopy
 361 also in cellular membranes of live cells at low temperatures,
 362 indicating that the passive cell penetration process analogously
 363 involves membrane fusion.

364 Future work will be directed toward unraveling further
 365 molecular details of the cell penetration mechanism suggested
 366 in this discovery study. In the next step, we need to understand
 367 the interaction of cell penetrating peptides with biological

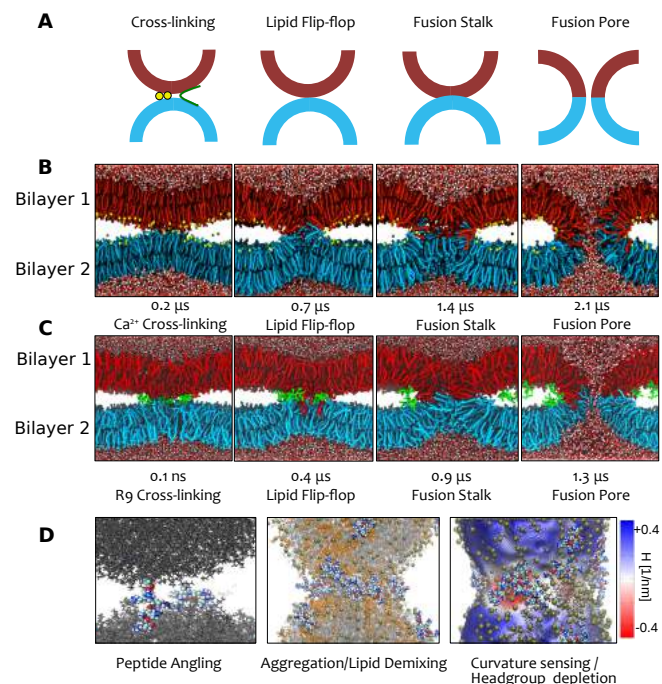


Fig. 5. A: Schematic drawing of vesicle fusion - lipid crosslinking, stalk initialization and subsequent onset of stalk formation through lipid flip-flop. **B:** Time evolution of the Ca^{2+} fusing bilayer system. **C:** Time evolution of the same system with R_9 . Cross section of systems undergoing fusion: crosslinking, flip-flop, fusion stalk, fusion pore. **D:** Driving forces of the mechanism. Peptide "angling" crosslinks vesicles and aggregates membranes, peptide agglomeration and lipid demixing create fusible interface, generation of negative curvature through strong binding to headgroups.

cell surfaces. Increased experimental understanding of the
 specific binding will allow us to develop more realistic models
 and vice versa. This will not only allow to firmly establish
 all the details of this hitherto unrecognized mechanism of
 passive cell penetration, but will also have a direct impact on
 development of smart cell delivery strategies for therapeutic
 molecules employing cell penetrating peptides. Should we get
 this passive cell penetration mechanism under full control, we
 may eventually be able to exploit it to directly deliver cargo
 into the cell without the need for releasing it from the transport
 vesicles, as is the case in active endocytosis.

Materials and Methods

Liposome Experiments. Leakage: Calcein containing vesicles were stirred at room temperature with LUV buffer in a quartz cuvette to obtain 1.5 ml of solution. The calcein fluorescence was monitored at 520 nm, with excitation at 495 nm. After an initial stirring phase of no less than 200 s, 3-6 μ l peptide in buffer solution was added. After the fluorescence intensity reached a plateau 50 μ l of TRITON-X were added. Fluorescence intensity measurements were performed on a Fluorolog-3 spectrofluorimeter (model FL3-11; JobinYvon Inc., Edison, NJ, USA) equipped with a xenon-arc lamp. See the SI Appendix for further details. **Confocal Microscopy:** GUVs labeled with DiD were prepared for confocal microscopy using electroformation in a 300 mOsm/l sucrose solution. Prepared GUVs were diluted with a glucose buffer (9 mM HEPES, pH 7.40 (KOH), 90 mM KCl, 90 mM EDTA, 120 mM glucose, 300 mOsm/l, filtrated) with 20 μ l 50 nM Atto 488 to a total volume of 300 μ l. Images were recorded using Olympus IX81 laser scanning confocal microscope (Olympus, Hamburg, Germany). For further details see the SI Appendix. **Cryoelectron Microscopy:** For cryo-EM sample preparation, 4 μ l of the sample were applied to plasma-cleaned EM grids (400 mesh copper grids, covered with Quantifoil film (R1.2/1.3)). Samples were plunge-frozen on the grids in liquid

402 Ethane in a Grid Plunger (Leica EM GP, Leica Microsystems
403 GmbH) with the following parameters: pre-blotting exposure 5 s,
404 blotting time 1.7 s, no post-blotting exposure. Chamber humidity
405 was set to 95% at 22 °C. The LUV solution was treated with R₉ (c
406 = 25 mM) in a ratio of 10:1 for t >60 s immediately before plunge
407 freezing. Cryo-electron micrographs were collected on a JEM-2100F
408 (JEOL Germany GmbH) operated at 200 kV (see the SI Appendix
409 for further details).

410 **Cell Experiments.** Forty thousand HeLa cells were seeded to a well of
411 μ -slide (ibiTreat; ibidi, Germany) 16-20 hours before the experiment.
412 Cells were washed with SF-DMEM and kept at 4 °C for 15 min
413 to inhibit endocytic processes. For treatment, pre-cooled (4 °C)
414 15 μ M solution of a peptide in SF-DMEM was added to cells
415 via media exchange and incubated for indicated periods of time
416 at 4 °C. In selected cases, cells were treated for 3 min with
417 a peptide at 4 °C, washed with pre-cooled SF-DMEM and further
418 incubated for indicated period of time at 4 °C in fresh SF-DMEM.
419 Cells were imaged using scanning confocal microscope (FluoView
420 1000, Olympus) and the tomograms we acquired on Titan Halo
421 transmission electron microscope (see the SI Appendix for details).

422 **Computational Details.** We use all atom molecular dynamics (MD)
423 for the fusion process: In a first setup, we created two curved
424 membranes via lipid population imbalances at the two leaflets of each
425 bilayer. In the second setup, we put a very small vesicle composed
426 of in the unit cell and let it fuse with its periodic image. Both of
427 these approaches facilitate formation of the stalk without enforcing
428 its shape. For calcium fusion we used optimized charge-scaled force
429 fields for ions, to account effectively for electronic polarization effects.
430 For vesicle aggregation and bifurcation calculations we employed
431 coarse-graining methods. See the SI Appendix for full details.

432 **ACKNOWLEDGMENTS.** P.Jun. acknowledges support from the
433 Czech Science Foundation (grant no. 16-01074S). C.A. thanks the
434 German Academic Exchange Service (DAAD) for support via a
435 P.R.I.M.E. fellowship and the Minerva foundation for a postdoc-
436 toral fellowship. A.M. acknowledges Magnus Ehrnrooth founda-
437 tion, Finland for funding. R.S. and M.H. acknowledge the Czech
438 Science Foundation (grant no. 17-03160S). Allocation of com-
439 puter time from the CSC Finland is appreciated. VH, RR and
440 CZ acknowledge the use of the cryoTEM in the Department of
441 Molecular Cell Anatomy, Univ. Regensburg, headed by Ralph
442 Witzgall. We acknowledge the Imaging Methods Core Facility at
443 BIOCEV, Faculty of Sciences, Charles University, institution sup-
444 ported by the Czech-BioImaging large RI project (LM2015062 and
445 CZ.02.1.01/0.0/0.0/16_013/0001775 funded by MEYS CR) for their
446 support with obtaining imaging data presented in this paper. We
447 thank Aleš Bendar and Markéta Dalecká, Mario Vazdar, Daniel
448 Harries, Šarka Pokorná, Uri Raviv, and Lea Fink for discussions
449 and technical assistance.

450 References

452 1. Bechara C, Sagan S (2013) Cell-penetrating peptides: 20 years later, where do we stand?
453 *FEBS Lett.* 587(12):1693–1702.
454 2. Wadia JS, Stan RV, Dowdy SF (2004) Transducible tat-ha fusogenic peptide enhances escape
455 of tat-fusion proteins after lipid raft macropinocytosis. *Nat. Med.* 10(3):310–315.
456 3. Pae J, et al. (2014) Translocation of cell-penetrating peptides across the plasma membrane is
457 controlled by cholesterol and microenvironment created by membranous proteins. *J. Control.*
458 *Release* 192(0):103–113.
459 4. Mishra A, et al. (2011) Translocation of hiv tat peptide and analogues induced by multiplexed
460 membrane and cytoskeletal interactions. *Proc. Natl. Acad. Sci. USA* 108(41):16883–16888.
461 5. Lamazière A, et al. (2007) Non-metabolic membrane tubulation and permeability induced by
462 bioactive peptides. *PLoS ONE* 2(2):e201.
463 6. Sun D, Forsman J, Lund M, Woodward CE (2014) Effect of arginine-rich cell penetrating
464 peptides on membrane pore formation and life-times: A molecular simulation study. *Phys.*
465 *Chem. Chem. Phys.* 16(38):20785–20795.
466 7. Hecce HD, Garcia AE, Cardoso MC (2014) Fundamental molecular mechanism for the cellular
467 uptake of guanidinium-rich molecules. *J. Am. Chem. Soc.* 136(50):17459–17467.
468 8. Ciobanasu C, Siebrasse JP, Kubitschek U (2010) Cell-Penetrating HIV1 TAT Peptides Can
469 Generate Pores in Model Membranes. *Biophys. J.* 99(1):153–162.
470 9. Zasloff M (2002) Antimicrobial peptides of multicellular organisms. *Nature* 415:389–395.
471 10. Lee MT, Sun TL, Hung WC, Huang HW (2013) Process of inducing pores in membranes by
472 melittin. *Proc. Natl. Acad. Sci. USA* 110(35):14243–14248.
473 11. Marks JR, Placone J, Hristova K, Wimley WC (2011) Spontaneous membrane-translocating
474 peptides by orthogonal high-throughput screening. *J. Am. Chem. Soc.* 133(23):8995–9004.
475 12. Guterstam P, et al. (2009) Elucidating cell-penetrating peptide mechanisms of action for mem-
476 brane interaction, cellular uptake, and translocation utilizing the hydrophobic counter-anion
477 pyrenebutyrate. *BBA - Biomembranes* 1788(12):2509–2517.

478 13. Manili O, Piao HR, Ayala-Sanmartin J (2014) Basic cell penetrating peptides induce plasma
479 membrane positive curvature, lipid domain separation and protein redistribution. *Int. J.*
480 *Biochem. Cell Biol.* 50(0):73–81.
481 14. Swiecicki JM, et al. (2015) Accumulation of cell-penetrating peptides in large unilamellar ves-
482 cles: A straightforward screening assay for investigating the internalization mechanism. *Pep-*
483 *tide Science* 104(5):533–543.
484 15. Katayama S, et al. (2013) Effects of pyrenebutyrate on the translocation of arginine-rich
485 cell-penetrating peptides through artificial membranes: Recruiting peptides to the mem-
486 branes, dissipating liquid-ordered phases, and inducing curvature. *BBA - Biomembranes*
487 1828(9):2134–2142.
488 16. Gestin M, Dowaidar M, Langel Ü (2017) *Uptake Mechanism of Cell-Penetrating Peptides*, eds.
489 Sunna A, Care A, Bergquist PL. (Springer International Publishing, Cham), pp. 255–264.
490 17. Chen YA, Scheller RH (2001) Snare-mediated membrane fusion. *Nat. Rev. Mol. Cell Biol.*
491 2(2):98–106.
492 18. Chen YA, Scales SJ, Patel SM, Doung YC, Scheller RH (1999) {SNARE} complex formation
493 is triggered by ca²⁺ and drives membrane fusion. *Cell* 97(2):165–174.
494 19. Babai N, Kochubey O, Keller D, Schneggenburger R (2014) An alien divalent ion reveals a ma-
495 jor role for ca²⁺ buffering in controlling slow transmitter release. *J. Neurosci.* 34(38):12622–
496 12635.
497 20. Papahadjopoulos D, Vail W, Pangborn W, Poste G (1976) Studies on membrane fusion. ii.
498 induction of fusion in pure phospholipid membranes by calcium ions and other divalent metals.
499 *Biochim. Biophys. Acta* 448(2):265–283.
500 21. Brock TG, Nagaprakash K, Margolis DI, Smolen JE (1994) Modeling degranulation with lipo-
501 somes: Effect of lipid composition on membrane fusion. *J. Memb. Biol.* 141(2):139–148.
502 22. Schneggenburger R, Rosenmund C (2015) Molecular mechanisms governing Ca²⁺ regula-
503 tion of evoked and spontaneous release. *Nat. Neurosci.* 18:935.
504 23. Kozlovsky Y, Kozlov MM (2002) Stalk model of membrane fusion: Solution of energy crisis.
505 *Biophys. J.* 82(2):882–895.
506 24. Zhao WD, et al. (2016) Hemi-fused structure mediates and controls fusion and fission in live
507 cells. *Nature* 534(7608):548–552.
508 25. Yang ST, Zaitseva E, Chernomordik LV, Melikov K (2010) Cell-penetrating peptide induces
509 leaky fusion of liposomes containing late endosome-specific anionic lipid. *Biophys. J.*
510 99(8):2525–2533.
511 26. Tünnemann G, et al. (2008) Live-cell analysis of cell penetration ability and toxicity of oligo-
512 arginines. *J. Peptide Sci.* 14(4):469–476.
513 27. Mitchell D, Steinman L, Kim D, Fathman C, Rothbard J (2000) Polyarginine enters cells more
514 efficiently than other polycationic homopolymers. *J. Peptide Res.* 56(5):318–325.
515 28. Hu Y, Sinha SK, Patel S (2015) Investigating hydrophilic pores in model lipid bilayers using
516 molecular simulations: Correlating bilayer properties with pore-formation thermodynamics.
517 *Langmuir* 31(24):6615–6631.
518 29. Churchward MA, et al. (2008) Specific lipids supply critical negative spontaneous cur-
519 vature—an essential component of native ca²⁺-triggered membrane fusion. *Biophys. J.*
520 94(10):3976–3986.
521 30. Düzgünes N, Wilschut J, Fraley R, Papahadjopoulos D (1981) Studies on the mechanism
522 of membrane fusion. role of head-group composition in calcium- and magnesium-induced
523 fusion of mixed phospholipid vesicles. *Biochim. Biophys. Acta* 642(1):182–195.
524 31. Summers S A, Guebert B A, Shanahan M F (1996) Polyphosphoinositide inclusion in artifi-
525 cial lipid bilayer vesicles promotes divalent cation-dependent membrane fusion. *Biophys. J.*
526 71(6):3199–3206.
527 32. Churchward MA, et al. (2008) Specific lipids supply critical negative spontaneous curva-
528 ture—an essential component of native ca²⁺-triggered membrane fusion. *Biophysical Journal*
529 94(10):3976–3986.
530 33. Kachar B, Fuller N, Rand R (1986) Morphological responses to calcium-induced interaction
531 of phosphatidylserine-containing vesicles. *Biophys. J.* 50(5):779–788.
532 34. Grafmüller A, Shillcock J, Lipowsky R (2007) Pathway of membrane fusion with two tension-
533 dependent energy barriers. *Phys. Rev. Lett.* 98(21):218101.
534 35. Marrink SJ, Mark AE (2003) The mechanism of vesicle fusion as revealed by molecular
535 dynamics simulations. *J. Am. Chem. Soc.* 125(37):11144–11145.
536 36. Noguchi H, Takasu M (2001) Fusion pathways of vesicles: A brownian dynamics simulation.
537 *J. Chem. Phys.* 115(20):9547–9551.
538 37. Fuhrmans M, Marrink SJ (2012) Molecular view of the role of fusion peptides in promoting
539 positive membrane curvature. *J. Am. Chem. Soc.* 134(3):1543–1552.
540 38. Derossi D, et al. (1996) Cell internalization of the third helix of the antennapedia homeo-
541 domain is receptor-independent. *J. Biol. Chem.* 271(30):18188–93.
542 39. Kawamoto S, et al. (2011) Inverted micelle formation of cell-penetrating peptide studied by
543 coarse-grained simulation: Importance of attractive force between cell-penetrating peptides
544 and lipid head group. *J. Chem. Phys.* 134(9):095103.
545 40. Siegel D P, Kozlov M M (2004) The Gaussian Curvature Elastic Modulus of N-
546 Monomethylated Dioleoylphosphatidylethanolamine: Relevance to Membrane Fusion and
547 Lipid Phase Behavior. *Biophys. J.* 87(1):366–374.
548 41. Hirose H, et al. (2012) Transient focal membrane deformation induced by arginine-rich pep-
549 tides leads to their direct penetration into cells. *Mol. Ther.* 20(5):984–993.
550 42. Kawamoto S, L. Klein M, Shinoda W (2015) Coarse-grained molecular dynamics study of
551 membrane fusion: Curvature effects on free energy barriers along the stalk mechanism. *J.*
552 *Chem. Phys.* 143:243112.
553 43. Nir S, Wilschut J, Bentz J (1982) The rate of fusion of phospholipid vesicles and the role of
554 bilayer curvature. *Biochim. Biophys. Acta* 688(1):275–278.
555 44. Robison AD, et al. (2016) Polyarginine interacts more strongly and cooperatively than poly-
556 lysine with phospholipid bilayers. *J. Phys. Chem. B* 120(35):9287–9296.
557 45. Allolio C, Haluts A, Harries D (2018) A local instantaneous surface method for extracting
558 membrane elastic moduli from simulation: Comparison with other strategies. *Chem. Phys.* in
559 press. 10.1016/j.chemphys.2018.03.004